Tuning Ferromagnetic Resonance via Disorder/Order Interfaces

Schneider, T.; Lenz, K.; Semisalova, A.; Gollwitzer, J.; Heitler-Klevans, J.; Potzger, K.; Fassbender, J.; Lindner, J.; Bali, R.;

Originally published:

May 2019

Journal of Applied Physics 125(2019), 195302

DOI: https://doi.org/10.1063/1.5088797

Tuning Ferromagnetic Resonance *via* Disorder/Order Interfaces

T. Schneider,[1,2] K. Lenz,[1] A. Semisalova,[1] J. Gollwitzer,[1] J. Heitler-Klevans,[1]K. Potzger,[1] J. Fassbender,[1,3] J. Lindner[1] and R. Bali[1,*]

[1]Helmholtz-Zentrum Dresden - Rossendorf, Institute of Ion Beam Physics and Materials Research, Bautzner Landstrasse 400, 01328 Dresden, Germany
[2]Department of Physics, Technische Universität Chemnitz, Reichenhainer Str. 70, 09126 Chemnitz, Germany
[3]Institute for Physics of Solids, Technische Universität Dresden, Zellescher Weg 16, 01069 Dresden, Germany

Abstract

Ferromagnetic resonance of a thin film alloy has been tuned by inducing lateral interfaces between layers differing in their lattice ordering and magnetic properties. By disordering B2 $Fe_{60}Al_{40}$ thin films to the A2 structure, thereby manifesting planar A2/B2 interfaces at selected depths, we show that the resonance lines at 10 GHz are shifted by 284 mT and 35 mT, for fields applied perpendicular-to-plane and in-plane, respectively. The resonance line-shift occurs over a broad frequency range, and is driven by strain relaxation due to the increasing magnetic layer thickness. A finer anomalous line shift occurs as the A2/B2 interface approaches the film/substrate interface prior to being removed from the film. The A2 structure can be re-annealed to B2 order, implying that disorder/order interface modification can provide a path for reversibly encoding resonant properties in alloy thin films.

Keywords: Interface effects, Ferromagnetic resonance, Disorder/Order interfaces

*Corresponding author, r.bali@hzdr.de

This manuscript was accepted by J. Appl. Phys. Click here to see the version of record.

Tunable ferromagnetic resonance behavior in magnetic materials can have applications in contactless sensing of encoded resonant lines for product tagging, similar to RFID. Other applications include magnonic devices, which employ spinwaves for data processing, where a tunable resonant behavior may be used for filtering and guiding spinwaves at mesoscopic scales.[1] Previous attempts to control the ferromagnetic resonance (FMR) response of thin films have involved several approaches, including fine-control of the film thickness,[2] intermixing in multilayers,[3] as well as alloying.[4] These modification paths demand a fine degree of control of the film growth parameters, and tend to result in irreversible shifts of the FMR lines, limiting their potential for applications.

Here we consider the case of B2 ordered lattices that act as non-ferromagnetic precursors, and where disordering leads to the onset of ferromagnetism. [5 – 12] Order/disorder transitions in $Fe_{60}Al_{40}$,[5 – 8] $Fe_{50}Rh_{50}$,[9 – 10] and $Fe_{60}V_{40}$,[11] can be exploited to sensitively tailor the saturation magnetization (M_S) through disorder. In the case of B2 $Fe_{60}Al_{40}$, disordering results in the formation of the A2 structure that can be induced by ion-irradiation. Energetic ions penetrate the lattice and randomize the atomic arrangement up to a film depth limited by the ion-energy. [7 – 8, 12] The limited ion depth penetration causes the formation of interfaces between the disordered and ordered material. We show that these disorder/order (A2/B2) interfaces have a profound influence on the resonant response. In particular the interfaces manifest large shifts of the resonance lines which are tunable *via* selection of their depth position within the film. The ion-energy acts as a lever for selecting the position of the lateral disorder/order interface. It has been shown that reversal from the A2 to the B2 structure can be achieved *via* thermal annealing, [5 – 12] and furthermore, laser pulsing can be used for disordering as well as reordering.[13] Thus, B2 ordered alloys can act as ion- and laser- compatible re-writable template for encoded magnetic patterns with signature responses to microwave excitations.

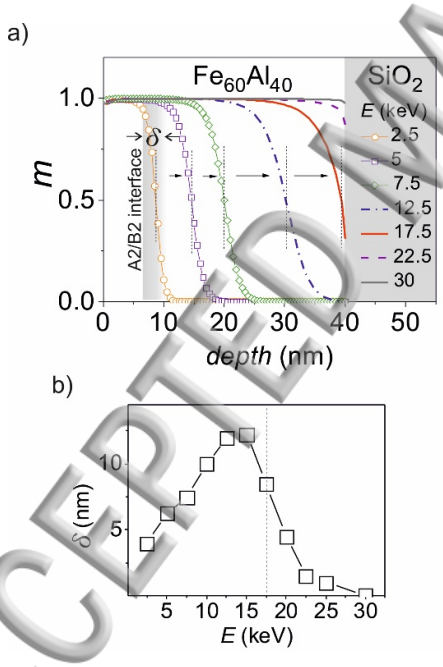

Figure 1: Depth dependence of the A2/B2 interface on the energy of the penetrating Ne^+ ions. (a) Semi-empirical prediction of the depth variation of the normalized magnetization, m, for Ne^+ irradiation at indicated ion-energy, E. The fluence applied in all cases is 6×10^{14} ions/cm^2. The dashed lines indicate the position of the A2/B2 interface, and δ is the interface width. **(b)** δ as a function of E. The dotted line at E = 17.5 keV represents the point where the A2/B2 and the $Fe_{60}Al_{40}/SiO_2$ interfaces coincide.

Until now, quasi-static observations have demonstrated a wide variation in the nucleation and growth of magnetic domains for films irradiated at different ion-energies.[14 – 15] Dynamic effects of the A2/B2 interface have been considered in case of non-uniform precession, suggesting that the interface acts as a spinwave pinning site.[16] However, for applications involving FMR detection, the relevant property is the magnetic anisotropy energy, that along with the M_S, determines the resonant precession and is highly susceptible to variations in the interface characteristics. Magnetic anisotropies may originate from differences in the lattice parameter of the A2 and B2 structures, [17 – 19] that may induce interfacial strain that relaxes with increasing thickness of the disordered layer. We show that a further contribution to the anisotropy arises from the localized

nanoscale deviations in the M_s prevalent at the interface as the structure transforms from the A2 to the B2 over a confined interfacial width.

We consider B2 $Fe_{60}Al_{40}$ films of 40 nm thickness as a model system, and introduce A2/B2 interfaces using energetic Ne^+ ions. The thin films preparation procedure as well as the magnetic properties of irradiated films have been reported previously.[7] A semi-empirical approach described in Ref. 7 can be used to predict the depth variation of M_s with ion-energy and fluence. The simulated displacements of atoms under ion-irradiation are integrated over the film thickness and compared with the experimentally observed magnetic properties, yielding a relationship between the atomic displacements and the induced M_s. The estimated depth-dependence of the normalized magnetization (m) in B2 $Fe_{60}Al_{40}$ films irradiated with Ne^+ ions at energy (E) varying from 2.5 to 30 keV is shown in Figure 1 (a).

The Ne^+-fluence in Figure 1 (a) has been kept fixed at 6×10^{14} ions cm^{-2}, for all E. This fluence has been selected such that the 40 nm thick B2 $Fe_{60}Al_{40}$ films used in this experiment can be fully magnetized, achieving a flat magnetization distribution, with M_s = 780 kA/m, for $E \geq 20$ keV. As E is lowered below 20 keV, the volume of the film possessing the maximum M_s (m = 1) recedes from the film/substrate interface. The film volume possessing m = 1 is of the disordered A2 structure, and as seen in Figure 1 (a), the A2/B2 interfaces correspond to the regions where m decays from 1 to 0.

A systematic shift of the A2/B2 interface depth, defined as the depth where m = 0.5, with increasing E is predicted (Figure 1(a)). For E = 7.5 and 17.5 keV, the interface lies at depths of 20 and 39.5 nm, respectively. Above 17.5 keV, the A2/B2 interface is pushed past the film/substrate interface, and is effectively removed, leaving a film possessing a nearly homogeneous M_s-distribution. Adjusting the ion-energy can therefore be used for positioning the A2/B2 interface at desired depths.

The interface width, δ, defined here as the width over which m decays from 0.95 to 0.05, has been plotted as a function of E in Figure 1(b). Increasing E not only shifts the position of the interface, but also varies δ. The highest δ of 12 nm occurs at E = 15 keV and as the interface is gradually expelled at higher ion-energies, δ decreases to 0. Even though δ is maximum at 15 keV, a particular point of interest is at E = 17.5 keV, where as seen in Figure 1(a), the A2/B2 region possesses a half-sigmoidal profile, and being positioned at a depth of nearly 40 nm, corresponds to the intersection of the A2/B2 and film/substrate interfaces.

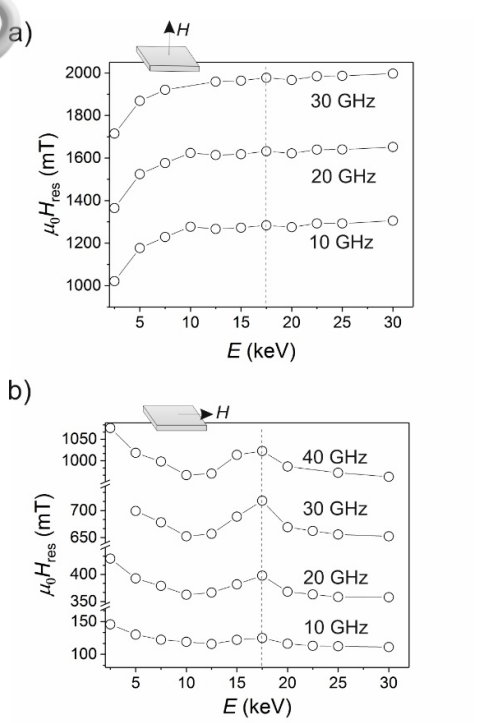

Figure 2: Dependence of the ferromagnetic resonance response of 40 nm thick $Fe_{60}Al_{40}$ films on the Ne^+ ion-irradiation energy, E. The dependence of the resonance field, H_{res} on the ion-energy is shown for **(a)** field perpendicular-to-plane and **(b)** in-plane geometry, respectively. The dotted line indicates the ion-energy at which the A2/B2 and the film/substrate interfaces coincide. The error in H_{res} determination is ± 0.1 mT.

Ferromagnetic resonance (FMR) spectra were measured for every E using a vector network analyzer. The sample was placed with the film in contact to a coplanar waveguide. The microwave transmission parameter S_{21} serves as the measured FMR signal. The excitation frequency, f, was kept fixed while the applied magnetic field was swept from 0 to 2 T to observe the resonance field, H_{res}. For each sample, four data sets were taken: the FMR spectra were measured for f = 2 to 40 GHz with the swept field oriented (i) perpendicular to the film-plane, as well as (ii) within the film plane. In addition the (iii) azimuthal and (iv) polar angular dependencies were recorded at a fixed frequency of 15 GHz. The resonance fields H_{res} were determined from fits of a complex Lorentzian to the FMR spectra (see Supplement for further details and Figures).

The shift in H_{res} with E at fixed frequencies is shown in Figures 2(a) and (b), for perpendicular and in-plane geometries, respectively. At 10 GHz, the difference in H_{res} for films irradiated at 2.5 and 30 keV is 284 mT with the field applied perpendicular-to-plane, and 35 mT with the field in-plane. Similar H_{res}-shifts are observed throughout the f-range.

As seen in Figure 2(a), with the field applied perpendicular to the film plane, the H_{res} increases with E and tends towards saturation above 10 keV. In case of in-plane field (Figure 2(b)), H_{res} decreases with increasing E and as in the previous case, the largest change occurs for E up to 10 keV. However, in the in-plane geometry, an anomalous H_{res} shift occurs at E = 17.5 keV (Figure 2(d)). Referring to Figure 1, this is the regime where the A2/B2 interface region of width δ approaches the film/substrate interface, and the two interfaces begin to coincide. This observed anomalous $H_{res}(E)$ dependence is not only useful for further tuning the FMR response, but also identifies the A2/B2 interface as the determining factor that causes the H_{res} shift.

The gradual increase of H_{res} with increasing E from 2.5 to 10 keV for fields perpendicular-to-plane (Figure 2(a)), points to the occurrence of an anisotropy contribution that favors an in-plane moment orientation, *i.e.* making the hard axis harder. This contribution tends to relax with increasing thickness of the ferromagnetic layer (due to increasing E, see Figure 1 (a)). Correspondingly, for the in-plane case in Fig. 2(b), the H_{res} decreases with increasing E, consistent with the decreasing anisotropy contribution. This inverse thickness-dependent behavior is known to occur in a variety of strained thin-film systems,[20] and is typically modelled using a second-order anisotropy contribution.

Conversely, the anomalous H_{res} shift at 17.5 keV, which occurs only for in-plane fields (Figure 2(b)) points to an additional anisotropy contribution, which is switched on as the A2/B2 interface begins to merge with the film/substrate interface, and switched off once the interface has been removed. This sensitive dependence of H_{res} on the interaction of the two interface types suggests that the effect originates from the inhomogeneous M_s prevalent in the interfacial region. Studies on nanometer scale spatial variations of the magnetization are rare. A case that is similar is that of surface roughness in thin films of homogeneous magnetization *i.e.*, occurrence of surface roughness can cause an additional contribution to the demagnetizing field, primarily due to local deviations of the moment orientation from the mean.[21 – 22] We attempt to model the variation of the demagnetizing field due to roughness-like effects, as a variation of a fourth-order anisotropy term, with a hard axis lying perpendicular to the film plane. [23]

From symmetry arguments, the net anisotropy energy density, K_{A2}, is assumed to be of the well-known form:

This manuscript was accepted by J. Appl. Phys. Click here to see the version of record.

$$K_{A2} = -K_{2\perp}\alpha_z^2 - \frac{1}{2}K_{4\perp}\alpha_z^4 \quad \ldots (1)$$

where the anisotropy constants, $K_{2\perp}$ and $K_{4\perp}$ represent the aforementioned second- and fourth-order anisotropy contributions, respectively, and α_x, α_y, and α_z are direction cosines.

Eq. (1) considers the anisotropy axes typically induced in a polycrystalline thin film. The the 2nd order $K_{2\perp}$ term models a uniaxial anisotropy, where the positive (negative) value refers to the easy (hard) axis being oriented along the sample's normal (z-axis). The 4th order anisotropy term, $K_{4\perp}$ acts as a correction to the 2nd order term and follows the same sign convention. Note that Eq. (1) neglects any in-plane anisotropy constant, consistent with the absence of any significant azimuthal variation of H_{res} in the measurements (Supplement).

The anisotropy constants can be determined by fitting the resonance equation to the data. The complete resonance condition that follows from Eq. (1) is given by:[24]

$$\left(\frac{\omega}{\gamma}\right)^2 = \left[\mu_0 H\eta_z - \cos 2\theta\left\{\mu_0 M_{\text{eff}} - \frac{K_{4\perp}}{M_s}\right\} + \frac{K_{4\perp}}{M_s}\cos 4\theta\right] \times \left[\mu_0 H\eta_z - \cos^2\theta\,(\mu_0 M_{\text{eff}}) + \frac{2K_{4\perp}}{M_s}\cos^4\theta\right] \quad \ldots(2)$$

$$\text{with } \eta_z = \sin\theta\sin\theta_H\cos(\varphi - \varphi_H) + \cos\theta\cos\theta_H \quad \ldots(3)$$

where, $\omega = 2\pi f$, γ denotes the gyromagnetic ratio, θ and φ define the magnetization direction in spherical coordinates, θ_H and φ_H fix the direction of applied field, H. An additional in-plane uniaxial anisotropy field, $K_{2\parallel}/M_s < 1$ mT that occurs in samples with $E > 22.5$ keV, has been neglected.

The resonance condition following from the above case, i.e. Eq. (2) & (3), has been applied to obtain the variation of the effective magnetization $\mu_0 M_{\text{eff}}$, the anisotropy fields $K_{2\perp}/M_s$ and $K_{4\perp}/M_s$ and the gyromagnetic ratio γ as a function of E. The fits were performed for all four measurement sets for each E to retrieve a matching set of parameters. The term $\mu_0 M_{\text{eff}} = \mu_0 M_s - 2K_{2\perp}/M_s$ as observed in FMR includes the shape anisotropy contribution $\mu_0 M_s$ that favors an in-plane magnetization orientation. Since $M_s(E)$ is known from magnetometry,[7] the resonance condition yields the respective anisotropy constants. Due to varying δ, the net M_s can show slight variations with E. However, for higher ion-energies, the fraction of the fully transitioned A2 region with the maximum M_s becomes much larger than that of the interfacial region, and for the estimation of anisotropy constants the M_s of the fully transformed A2 region will be applied.

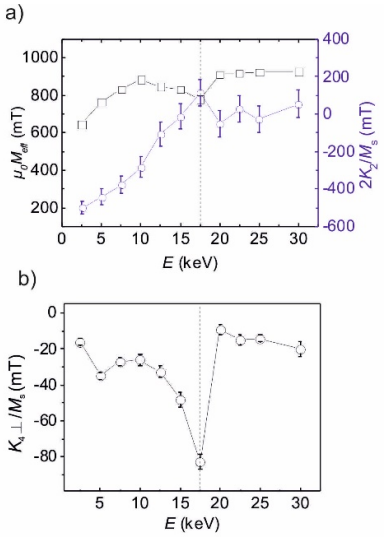

Figure 3: Dependence of film properties on the Ne^+ ion-energy, E. (a) $\mu_0 M_{\text{eff}}$ (black squares) and the second-order $K_{2\perp}$ (blue circles) and **(b)** fourth-order anisotropy term, $K_{4\perp}$. The dotted line indicates the predicted coincidence of the A2/B2 and the film/substrate interfaces.

First we consider the variations of the anisotropy fields with E. Figure 3(a) shows the variation of $\mu_0 M_{\text{eff}}$ and $2K_{2\perp}/M_s$ with E. It is seen that although negative $2K_{2\perp}/M_s$ values are observed for $E \leq 17$ keV, the magnitude is not sufficient to overcome the in-plane shape anisotropy (since $\mu_0 M_{\text{eff}}$ remains positive). Therefore the net easy axis for all samples lies within the film plane. For $E < 17$ keV, $K_{2\perp}$ is negative and decays with increasing E, *i.e.* with

increasing depth of the A2/B2 interface, implying a decaying anisotropy. A sign-reversal to a small negative $2K_{2\perp}/M_s$ occurs for E = 17.5 keV, above which $2K_{2\perp}/M_s$ fluctuates around zero.

In all cases it is necessary to consider the 4th order term to achieve satisfactory data fits of the polar angular variation of H_{res} (see Figure S6 of the supplement). The variation of $K_{4\perp}$ is shown in Figure 3(b), in the form of the anisotropy field $K_{4\perp}/M_s$. The fourth-order anisotropy field stays approximately constant at -30 mT for E < 10 keV and at -20 mT for E > 20 keV. In the region between 15 and 20 keV, corresponding to the hump seen in the $H_{res}(E)$ of Figure 2(b), $K_{4\perp}/M_s$ shows a significant spike down to -82 mT at E = 17.5 keV.

It is clear from Figure 3, that the value of E = 17.5 keV, where the A2/B2 interface intersects with the film/substrate interface is also critical for the anisotropy constants—here, $K_{2\perp}$ undergoes a sign-reversal and $K_{4\perp}$ shows a maximum.

The net effect of $K_{2\perp}$ and $K_{4\perp}$ can be better understood by using Eq. (1) to plot the anisotropy energy surfaces of K_{A2}, shown for three cases *viz.* E = 7.5, 17.5, and 25 keV in Figures 4(a) to (c). For E = 7.5 keV, disregarding the shape anisotropy, $K_{2\perp}$ (= -146.8 kJ/m^3) favors an in-plane moment orientation, and strengthens the in-plane easy axis originating from $K_{4\perp}$ (= –21.1 kJ/m^3). The net anisotropy energy surface possesses an easy plane. At E = 17.5, $K_{2\perp}$ is largely relaxed, undergoing a sign-reversal as well as a reduction in magnitude to +43.8 kJ/m^3. In contrast, $K_{4\perp}$ shows a spike to –64.4 kJ/m^3, giving a net anisotropy energy surface with a slight tendency for the magnetization to tilt out of the film plane (Figure 4(b)). At E = 30 keV, where the film magnetization is largely homogeneous, both $K_{2\perp}$ (+21.1 kJ/m^3) as well as $K_{4\perp}$ (–12.2 kJ/m^3) are largely diminished and result in an approximately isotropic K_{A2}-variation (Figure 4(c)). In the regime where the A2/B2 and the film/substrate interfaces overlap, the $K_{2\perp}$ can fluctuate around zero, sensitively varying the anisotropy energy surface.

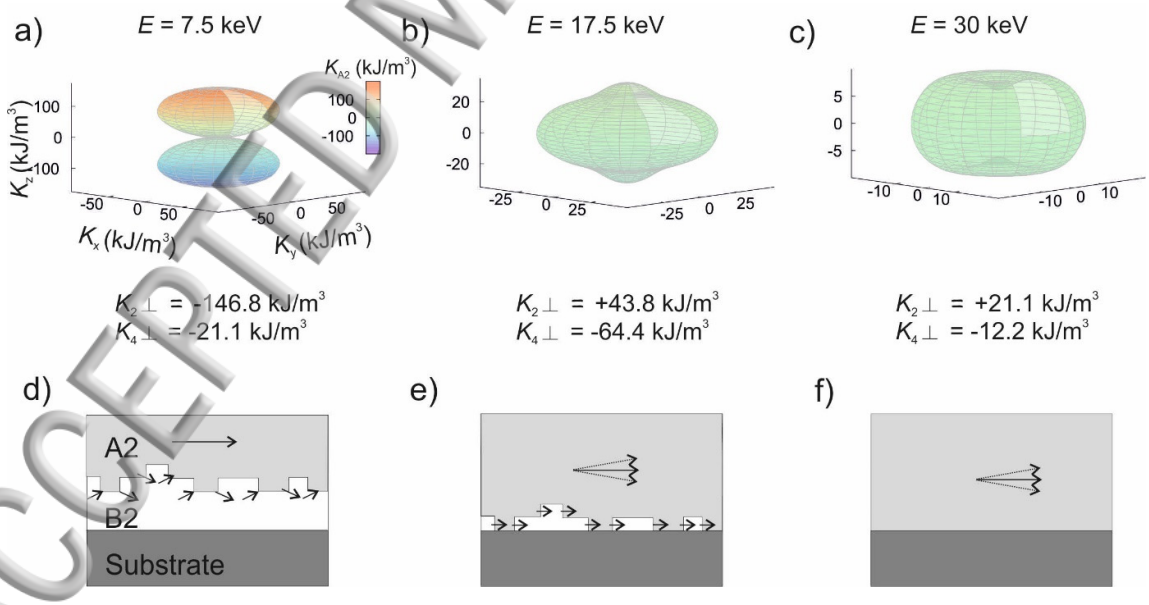

Figure 4: Anisotropy energy surfaces for the net anisotropy, K_{A2}, for selected A2/B2 interface depths manifested by varying the ion-energy, E. (a) The interface positioned within the film, after Ne^+ irradiation at E = 7.5 keV **(b)** colliding with the film/substrate interface (E = 17.5 keV), and **(c)** after interface expulsion (E = 30 keV), **(d-e)** schematic sketches of the A2/B2 interface positions corresponding to (a-c) respectively. Note that the anisotropy energy surfaces in (a – c) do not consider the shape anisotropy.

The monotonic decay of the $K_{2\perp}$ with increasing E, and hence increasing magnetic thickness, strongly suggests an interfacial origin of the anisotropy term. The known lattice

expansion of the A2 region can be expected to induce strain at the A2/B2 interface.[18 - 19] The increased effective thickness of the A2 layer at higher E allows the relaxation of this strain along the perpendicular axis, resulting in the decaying $K_{2\perp}$. The nearly-zero $K_{2\perp}$ term in the absence of the A2/B2 interface shows that the A2 $Fe_{60}Al_{40}$ is fully relaxed when interfaced with the amorphous SiO_2 surface. Our results show that the anisotropy induced from the lattice expansion tends to align the magnetization to lie within the film plane.

The A2/B2 interfacial roughness further increases the tendency for in-plane magnetization alignment. In contrast to $K_{2\perp}$, the $K_{4\perp}$ term remains largely constant with varying A2/B2 interface depth. However, $K_{4\perp}$ appears to be sensitive to δ, and particularly to the confinement of the A2/B2 region for E = 17.5 keV. This is consistent with the ansatz that $K_{4\perp}$ emerges from the roughness-like inhomogeneity of the A2/B2 interface. The magnetically rough region consisting of decaying M_s can be expected to possess magnetostatically coupled high density point charges. The confined width δ, and the homogeneously magnetized A2 region above it, acting as a macrospin, forces an additional in-plane anisotropy contribution.

The effect of the anisotropy energy surfaces on the magnetization is schematically depicted in Figure 4(d) – (f). For the E = 7.5 keV the moments that are confined within δ can possess a degree of freedom to incline away from the film plane. This angular degree of freedom is suppressed at E = 17.5 keV, when the interface merges into the SiO_2 substrate, increasing confinement of the moments to the film plane, thereby increasing $K_{4\perp}$. Further increase in E results in lowered $K_{4\perp}$, which nevertheless remains non-zero and negative, likely due to inherent roughness of the SiO_2 substrate.

The $K_{2\perp}$ which originates form the continuous A2 layer forming the macrospin behaves differently to the $K_{4\perp}$. At lower E, say 7.5 keV, $K_{2\perp}$ is relatively high and confines the macrospin of the continuous A2 layer to lie within the film plane. With increasing E, the magnetic thickness and relaxing strain, the macrospin is allowed to incline out of the film plane, as shown in Figure 4(e) and (f). The varying tendency for planar confinement of the interfacial moments and the macrospin results in the shifting H_{res}, leading to the tunable FMR response.

In conclusion, the anisotropy energy surfaces in alloys possessing disorder/order interfaces can be engineered by adjusting the depth of the interface, thereby tuning the resonant fields over a broad frequency range. Disorder is generated using energetic ions, where the ion energy can be selected to determine the depth of the disorder/order interface. Anisotropy contributions are induced due to the lattice mismatch between disordered and ordered layers as well as the magnetically inhomogeneous interfacial region. The disorder is thermally reversible, thereby allowing for encoding resonant responses in thin film alloys in a reprogrammable way. This work may instigate the investigation of this phenomenon in other binary alloys possessing disorder induced ferromagnetic onsets.

Supplementary Material

Selected Ferromagnetic Resonance Spectra, along with frequency and angular dependence of the resonance fields and diagnostics are provided.

Acknowledgments

This work was funded by the Deutsche Forschungsgemeinschaft (Grant BA 5656/1-1). The irradiation experiments were performed at the Ion beam Centre of the Helmholtz-Zentrum Dresden-Rossendorf.

References

[1] M. Krawczyk and D. Grundler, J. Phys.: Cond. Matter **26**, 123202 (2014).
[2] S. Azzawi, A. Ganguly, M. Tokac¸, R. M. Rowan-Robinson, J. Sinha, A. T. Hindmarch, A. Barman, and D. Atkinson, Phys. Rev. **B** 93, 054402 (2016).
[3] J.-M. L. Beaujour, A. D. Kent, D. Ravelosona, I. Tudosa, and E. E. Fullerton, J. Appl. Phys. **109**, 033917 (2011).
[4] B. Obry, T. Meyer, P. Pirro, T. Brächer, B. Läge, J. Osten, T. Strache, J. Fassbender, and B. Hillebrands, Appl. Phys. Lett. **102**, 022409 (2013).
[5] A. J. Bradley and A. H. Jay, Proc. R. Soc., Ser. A **136**, 210 (1932).
[6] P. A. Beck, Metallurgical and Materials Transactions B **2**, 2015 (1971).
[7] R. Bali, S. Wintz, F. Meutzner, R. Hübner, R. Boucher, A. A. Ünal, S. Valencia, A. Neudert, K. Potzger, J. Bauch, F. Kronast, S. Facsko, J. Lindner, and J. Fassbender, Nano Lett. **14**, 435 (2014).
[8] F. Röder, G. Hlawacek, S. Wintz, R. Hübner, L. Bischoff, H. Lichte, K. Potzger, J. Lindner, J. Fassbender, R. Bali, Sci. Rep. **5**, 16786 (2015).
[9] S. Kosugi, T. Matsui, N. Ishikawa, M. Itou, Y. Sakurai, K. Aikoh, K. Shimizu, Y. Tahara, F. Hori, A. Iwase, J. Appl. Phys. **109**, 07B737 (2011).
[10] A. Heidarian, R. Bali, J. Grenzer, R. Wilhelm, R. Heller, O. Yildirim, J. Lindner, and K. Potzger, Nucl. Instrum. Methods Phys. Res., Sect. B **358**, 251 (2015).
[11] T. Devolder, T. Tahmasebi, S. Eimer, T. Hauet, and S. Andrieu, Appl. Phys. Lett. **103**, 242410 (2013).
[12] J. Fassbender, M. O. Liedke, T. Strache, W. Möller, E. Menendez, J. Sort, K. V. Rao, S. C. Deevi, J. Nogues, Phys. Rev. B **77**, 174430 (2008).
[13] J. Ehrler, M. He, M. V. Shugaev, N. I. Polushkin, S. Wintz, V. Liersch, S. Cornelius, R. Hübner, K. Potzger, J. Lindner, J. Fassbender, A. A. Ünal, S. Valencia, F. Kronast, L. V. Zhigilei, and R. Bali, *ACS Appl. Mater. Interfaces* **10**, 17, 15232–15239 (2018).
[14] N. Tahir, R. Gieniusz, A. Maziewski, R. Bali, K. Potzger, J. Lindner, J. Fassbender, Opt. Express **23** (13), 16575-16581 (2015).
[15] N. Tahir, R. Gieniusz, A. Maziewski, R. Bali, M. P Kostylev, S. Wintz, H. Schultheiss, S. Facsko, K. Potzger, J. Lindner, J. Fassbender, IEEE Trans. Magn. **50** (11), 6101304 (2014).
[16] N. Tahir, R. Bali, R. Gieniusz, S. Mamica, J. Gollwitzer, T. Schneider, K. Lenz, K. Potzger, J. Lindner, M. Krawczyk, J. Fassbender, A. Maziewski, Phys. Rev. B **92** (14), 144429 (2015).
[17] L. E. Zamora, G. A. Pérez Alcázar, G. Y. Vélez, J. D. Betancur, J. F. Marco, J. J. Romero, A. Martínez, F. J. Palomares, J. M. González, Phys. Rev. B **79**, 094418 (2009).
[18] A. Hernando, X. Amils, J. Nogues, S. Surinach, M. D. Baro, and M. R. Ibarra, Phys. Rev. B **58**, R11864 (1998).
[19] E. Menéndez, J. Sort, M. O. Liedke, J. Fassbender, S. Suriñach, M. D. Baró, J. Nogués, New J. Phys. **10**, 103030 (2008).
[20] M.T. Johnson, P.J.H. Bloemen, F.J.A. den Broeder, J.J. de Vries, Rep. Prog. Phys. **59**, 1409 (1996).
[21] B. Heinrich, T. Monchesky, R. Urban, J. Magn. Magn. Mater. **236**, 3, 339 (2001).
[22] M. Li and G.-C. Wang, J. Appl. Phys. **83**, 5313 (1998).
[23] J. B. Mohammadi, K. Cole, T. Mewes, C. K. A. Mewes, Phys. Rev. B **97**, 014434 (2018).
[24] K. Lenz, E. Kosubek, K. Baberschke, H. Wende, J. Herfort, H.-P. Schönherr, K. H. Ploog, Phys. Rev. B **72**, 144411 (2005).

a)

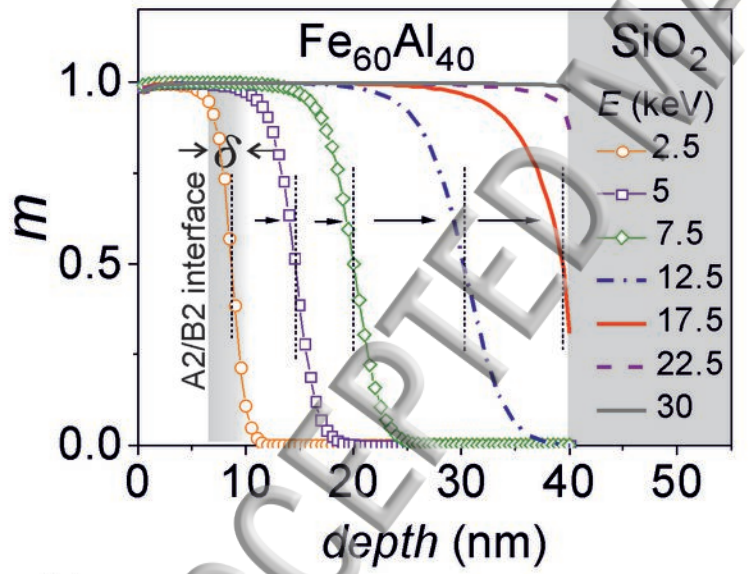

b)

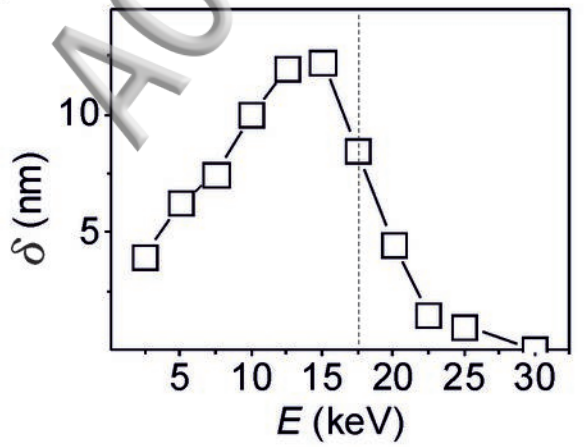

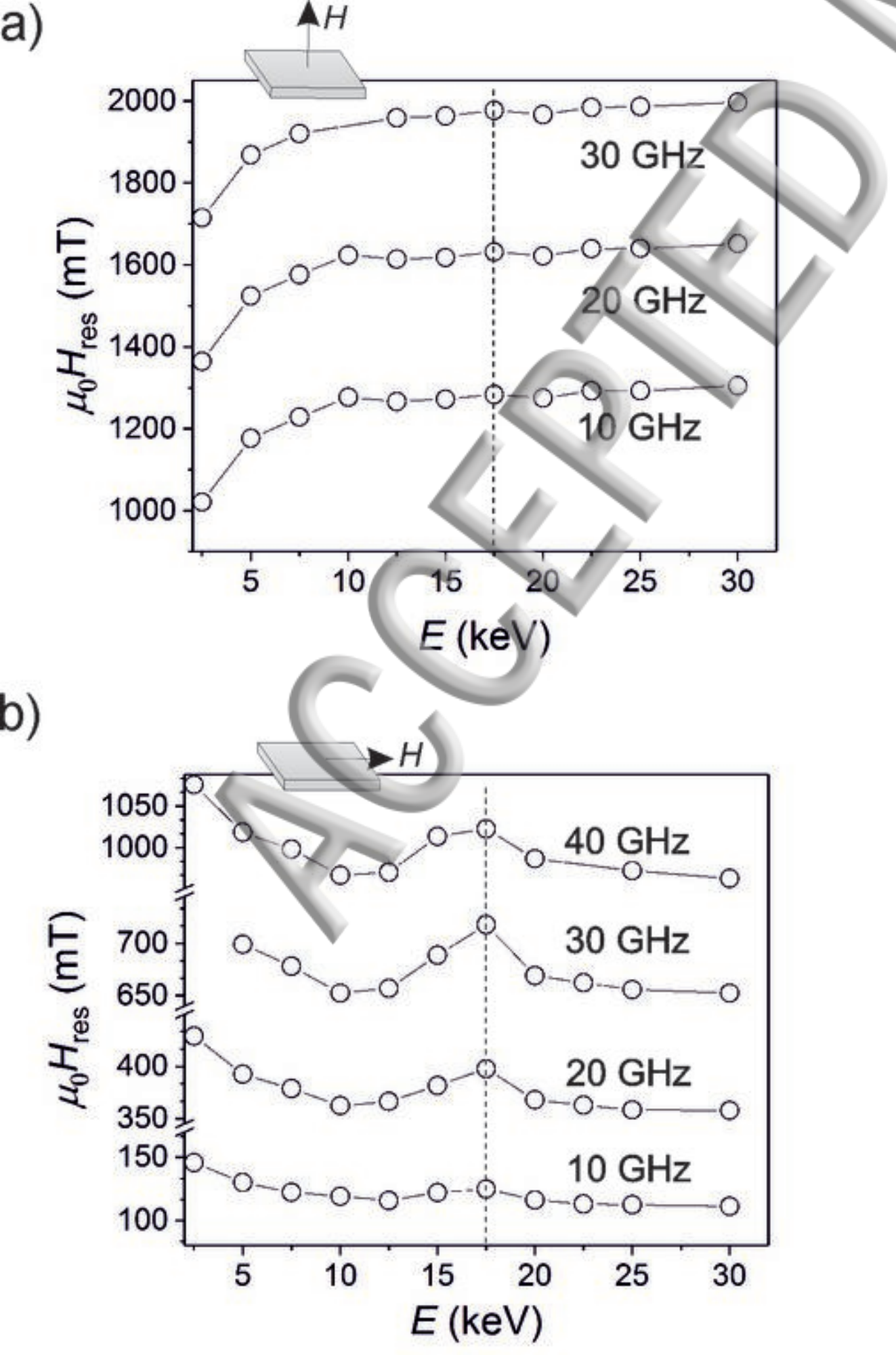
a)
H
2000
1800
1600
1400
1200
1000
$\mu_0 H_{res}$ (mT)
30 GHz
20 GHz
10 GHz
5
10
15
20
25
30
E (keV)
b)
H
1050
1000
700
650
400
350
150
100
$\mu_0 H_{res}$ (mT)
40 GHz
30 GHz
20 GHz
10 GHz
5
10
15
20
25
30
E (keV)

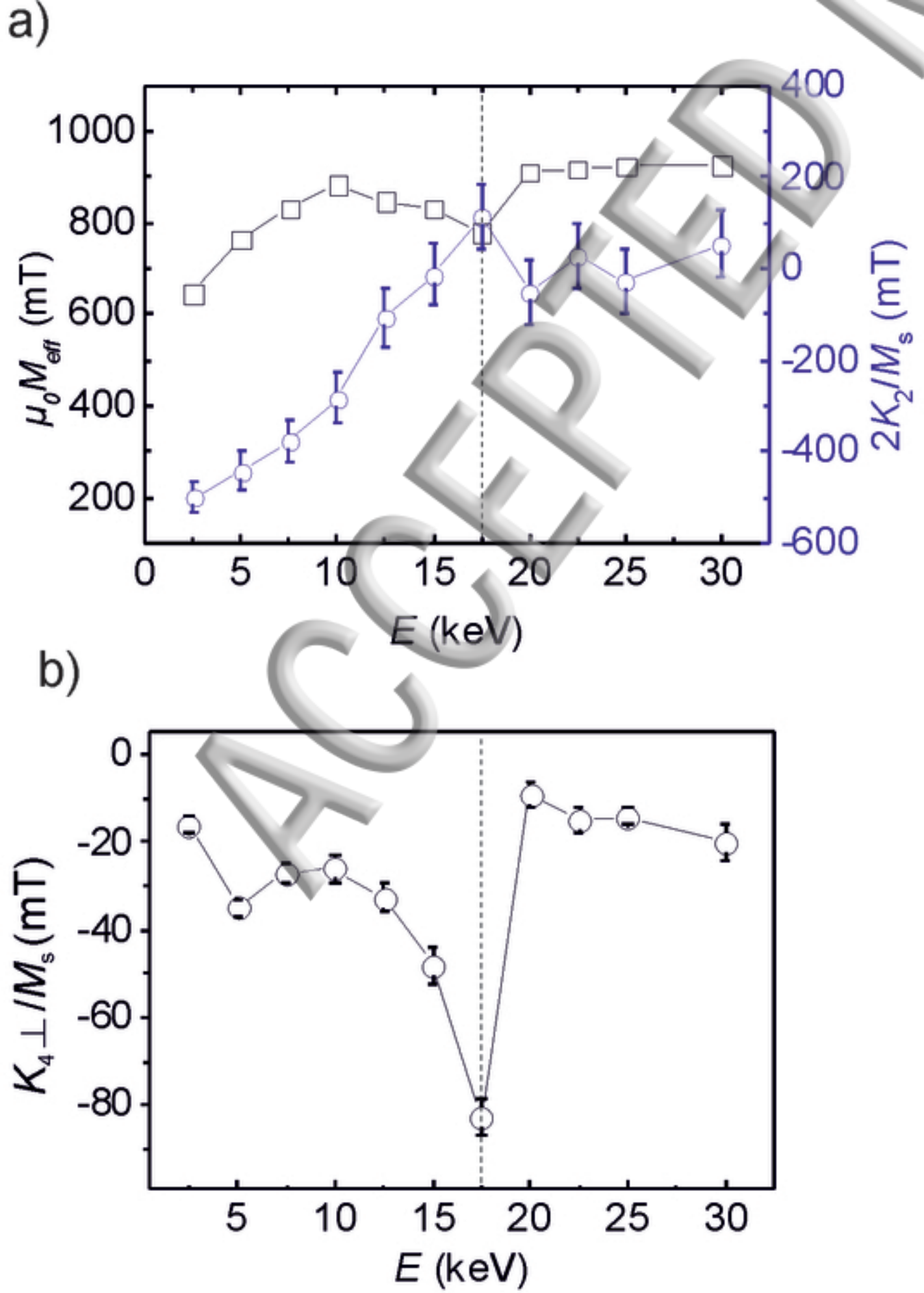
a)
1000
800
600
400
200
$\mu_0 M_{eff}$ (mT)
400
200
0
-200
-400
-600
$2K_2/M_s$ (mT)
0
5
10
15
20
25
30
E (keV)
b)
0
-20
-40
-60
-80
$K_4\perp/M_s$ (mT)
5
10
15
20
25
30
E (keV)

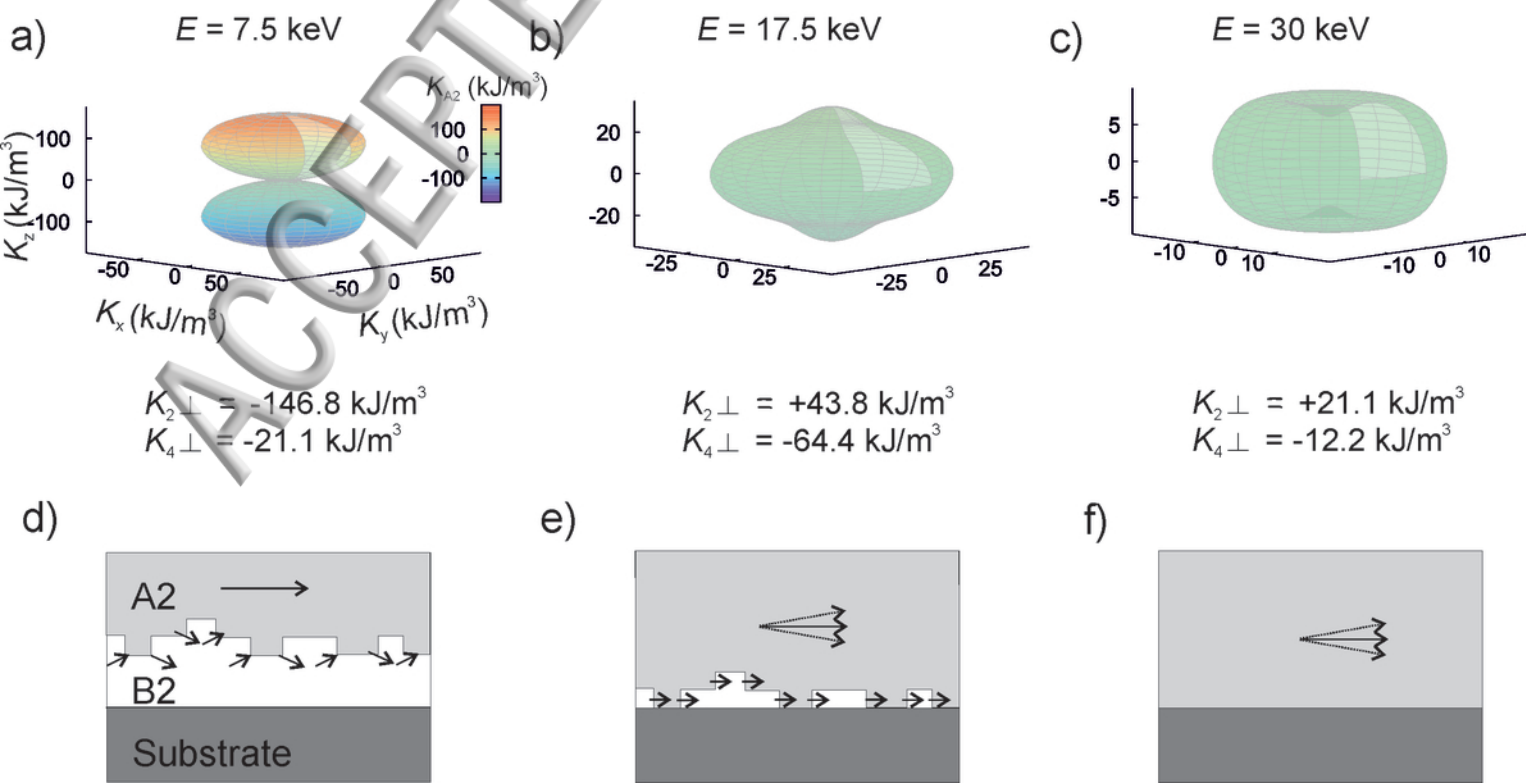
a)
E = 7.5 keV
K_A2 (kJ/m^3)
100
0
-100
K_z (kJ/m^3)
100
0
-100
-50
0
50
K_x (kJ/m^3)
-50
0
50
K_y (kJ/m^3)
K_2⊥ = -146.8 kJ/m^3
K_4⊥ = -21.1 kJ/m^3
b)
E = 17.5 keV
20
0
-20
-25
0
25
-25
0
25
K_2⊥ = +43.8 kJ/m^3
K_4⊥ = -64.4 kJ/m^3
c)
E = 30 keV
5
0
-5
-10
0
10
-10
0
10
K_2⊥ = +21.1 kJ/m^3
K_4⊥ = -12.2 kJ/m^3
d)
A2
B2
Substrate
e)
f)